Pergamon

Cement and Concrete Research, Vol. 25, No. 1, pp. 147-156, 1995

0008-8846/95 $9.50+.00

0008-8846(94)00122-7

THE FRACTAL ARRANGEMENT OF HYDRATED CEMENT PASTE

Douglas Winslow
School of Civil Engineering
Purdue University, West Lafayette, Indiana

and

John M. Bukowski and J. Francis Young
Center for Cement Composite Materials
University of Illinois, Urbana, Illinois

(Refereed)
(Received February 3; in final form September 29, 1994)

ABSTRACT

Data from small-angle X-ray scattering experiments are used to determine the fractal types and dimensions of hydrated portland cement pastes over a range of length scales. The larger-scale, 200-1500 Å, geometry at most degrees of water saturation is found to be that of a rough surface fractal. The smaller-scale, 30-200 Å, geometry is found to be a mass fractal in saturated pastes. This geometry changes gradually with drying, and becomes a rough surface fractal at saturations less than about 50%. Completely oven dried pastes are found to have a considerably altered geometry.

INTRODUCTION

When a beam of radiation passes through a material, some of the radiation will be scattered. This scatter is particularly noticeable at small angles, i.e. close to the incident beam. A good general introduction to subject is reference [1] The details of the angular dependence of the intensity of the scattered radiation can provide a variety of microstructural information about the material.

Prominent among this information is the specific surface area and the radius of gyration of the entities that are responsible for the scatter within the material. Recently, researchers have begun to obtain information on the fractal geometry of the microstructure. It is the purpose of this paper to report findings regarding changes in the fractal geometry of hydrated cement paste as deduced from scattering.

In small-angle scattering research, the scattering angle, Θ, may be defined as the total angle between the incident beam and the scattered radiation. It is common to convert this angle to a related parameter, the scattering vector Q, via the following relation:

$$Q = \frac{4\pi \sin(\Theta/2)}{\lambda} \tag{1}$$

where λ is the wavelength of the incident radiation. It is seen that Q is another angular parameter, related to the scattering angle Θ, but placed on a unit wave-length basis. Q, like Θ, is inversely proportional to the size, or spacing, of a material's features that give rise to the scatter. Scatter from larger features occurs at smaller values of Θ and Q, and scatter from smaller features appears at larger Q. The relationship[2] between the size of a feature and its corresponding Q is given by:

$$\text{feature size} = \frac{2\pi}{Q} \tag{2}$$

If one prepares a log-log plot of scattered radiation intensity vs Q, one frequently obtains a linear result over a reasonably wide angular range. The slope of such a straight line region gives information on the fractal nature of the scattering material. A good review of the subject is given by Schmidt[3].

Among the possible slopes that such a log-log plot could have, there are two important ranges of slopes of particular interest here. These are shown in Figure 1.

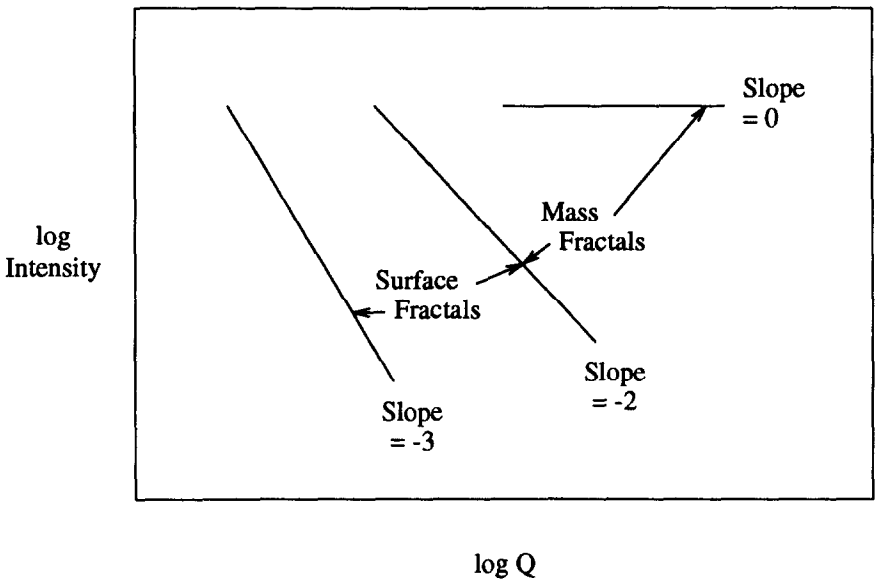

Figure 1 - Important Ranges of Slopes

One range includes all slopes between -3 and -2. Scatter that produces plots falling into this category comes from surface fractals. When the incident beam of radiation has been collimated as a slit, the fractal dimension of these surfaces is given by:

$$D = 5 + \text{SLOPE} \tag{3}$$

(A slightly different equation is needed for pinhole collimation.)

The second range covers slopes between -2 and 0. Scatter in this range comes from mass fractals, and, for slit collimation, their dimension is given by:

$$D = 1 - \text{SLOPE} \tag{4}$$

Mass fractals are frequently, but not necessarily, formed by aggregations of small subunits. Their distinguishing characteristic is that their mass, or volume, that may be enclosed in a sphere varies in proportion to a power of the radius of that sphere. That power is the fractal dimension of the mass fractal. A "two-dimensional" object such as a large, thin plate has a mass fractal dimension of 2. A space-filling, solid has a mass fractal dimension of 3. Porous objects, that are also mass fractals, tend to have dimensions between 2 and 3.

A surface fractal is a surface, or interface, having an area that is proportional to a power of the size of the device used to measure that area. A smooth surface has a surface fractal dimension of 2. A surface that is so irregular and convoluted that it fills space has a surface fractal dimension of 3. Thus, the dimension 3 is seen to be a meeting point where sufficiently irregular surface fractals and sufficiently dense mass fractals both become space filling, and indistinguishable.

EXPERIMENTAL MATTERS

The research reported here was carried out at the Robert R. Wilson Synchrotron Laboratory at Cornell University. The synchrotron emits intense X radiation that was used for the scattering. The experimental arrangement was straightforward, and is shown schematically in Figure 2.

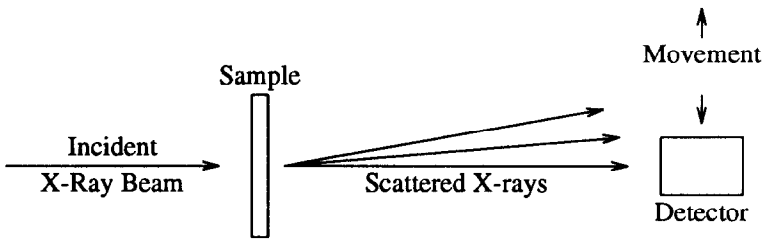

Figure 2 - Schematic of X-Ray Scattering Arrangement (not to scale)

The radiation first passes through a monocrometer that selects the desired wavelength. For this study a wave length of 0.071 nm (0.71 Å, i.e. MoK_{α}) was used because this permits the sample to be of reasonable thickness. The monochromatic radiation then passes through a series of slits that form it into a beam with a rectangular cross section about 0.25 mm × 20 mm.

The beam then passes through the sample that is positioned at right angles to the radiation. The sample is contained in a holder with Mylar windows. The scattered X-rays are detected by an ionization counter, with its own defining slits, located 500 mm down-stream from the sample. The detector is sequentially stepped along a path at right angles to the X-ray beam, and the intensities at various angles are recorded. The angular resolution of the set-up used here was 0.02°. Intensities were recorded over an angular range from 0° to about 2°. This range converts

to Q values over a useful range from about 0.003 $Å^{-1}$ to 0.3 $Å^{-1}$, i.e. about 2 orders of magnitude.

The intensities were recorded with a maximum error of ± 2% at about 30 angular positions within the experimental range. In addition, the scatter from the experimental apparatus itself, the so-called parasitic scatter, was determined during each experiment. This was used to correct the measured scatter so that the corrected values were only the scatter from the sample itself. It took 10-15 minutes to obtain a complete set of data for a single sample. Replicate tests were performed on the same sample in most instances, and no significant differences were observed between the duplicates.

The samples were all made from an ASTM Type I portland cement mixed at a w/c = 0.4 under ambient conditions. The samples were cast as thin rectangular prisms with dimensions of about 10 mm × 30 mm × 1 mm. The samples were removed from their molds about 1 day after they were mixed and were placed in $Ca(OH)_2$-saturated water to continue hydration at room temperature. All samples tested in this study hydrated for 28 days.

After 28 days, many of the samples were conditioned to water contents less than 100% saturation. This was done by equilibration with relative humidities less than 100%. Some samples were oven-dried prior to equilibration and, hence, *ad*sorbed water vapor. Other samples began equilibration from the saturated state and, hence, *de*sorbed water vapor. Finally, some samples were left in the 100% saturated state, and others were completely oven dried. The saturated samples were considered to have a degree of saturation of 100%, and the oven-dried samples a degree of saturation of 0%. After the scattering experiments were complete, all samples were oven dried at 105° C, and the amount of evaporated water per dry gram of paste determined. This was used to calculate their degrees of saturation.

RESULTS

The logarithms of the scattered intensities from each sample were plotted against the logarithims of the corresponding Q values to form plots such as the typical examples in Figure 3. All such plots in this study had two nearly linear regions that, combined, included all the data that were gathered. The slopes in the smaller-Q region varied only slightly for samples with widely differing degrees of saturation. The slopes in the larger-Q region changed much more with degree of saturation. The wetter samples had less steep the slopes.

The slopes of each linear region were determined by linear regression. Table 1 contains the slopes for each region and sample that was tested. It also contains the water contents of each sample, and is arranged in order of increasing degree of saturation. Finally, Table 1 lists the values of Q that bound each linear region for each sample. The minimum and intermediate Q are associated with the two sizes that bound the smaller-Q fractal region. And, the intermediate and maximum Q values bound the larger-Q region.

DISCUSSION and CONCLUSIONS

Larger-Scale Geometry

The slopes from the scatter generated by the larger-scale, (smaller Q) features of the pastes are given in the 3rd column of Table 1. It is seen that the oven dried samples have slopes associated with mass fractals, i.e. slopes between 0 and -2. The samples with greater degrees of

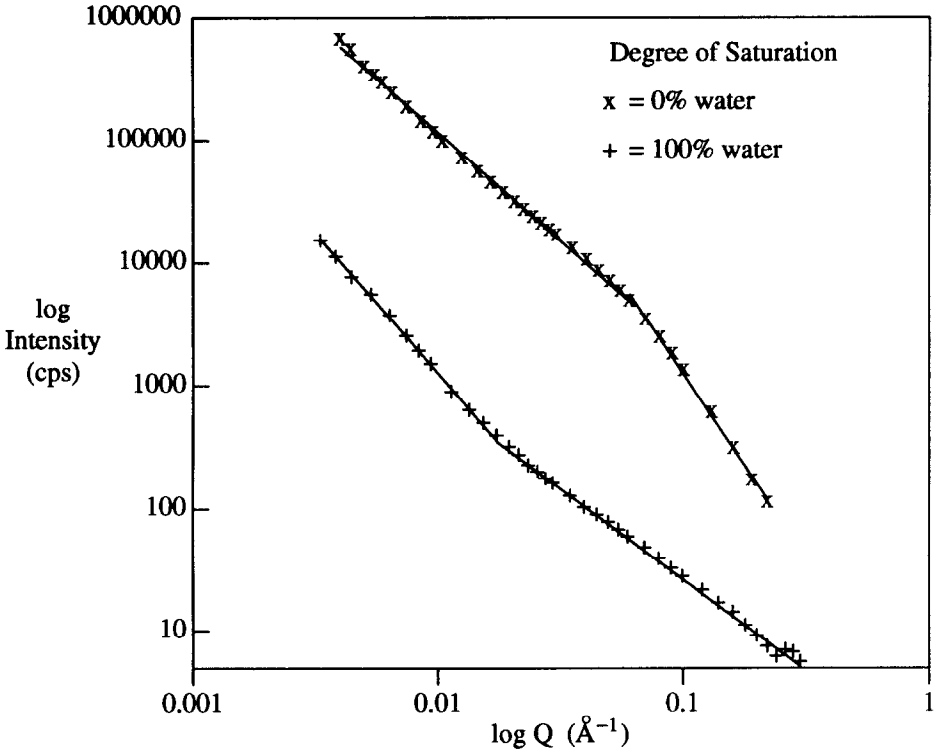

Figure 3 - Typical Results in a log-log Plot

saturation all have slopes associated with surface fractals, i.e. slopes between -2 and -3. Thus, Equation 4 must be used to find the fractal dimensions of the oven dried samples, while Equation 3 can be used for the others. Figure 4 shows the resulting fractal dimensions, and fractal types, of the larger-scale features of the pastes.

Figure 4 indicates that, except for the oven dried pastes, the larger-scale geometry is characterized by a solid having a surface that is fractal. And, this surface is quite rough with fractal dimensions ranging from 2.5 to 3.0. The range in sizes over which this fractal surface geometry extends can be found from the limiting Q values in Table 1. The intermediate Q values, excepting the oven dried ones, vary about 0.03 Å^{-1}, and the minimum Q values about 0.004 Å^{-1}. That is, the Q values span about an order of magnitude. These Q's translate via Equation 2 to a range of sizes of about 200-1500 Å.

The true upper limit for these larger-scale features may be greater than 1500 Å. This is because the experimental limit is fixed by the smallest Q, or angle, at which data can be gathered. This smallest angle is controlled by the incident beam width. If a narrower beam had been used, data from smaller angles would be available. Such data might show that the fractal regime extends to even smaller Q. Thus, the upper limit of the surface feature size that is fractal may be greater than 1500 Å.

Smaller-Scale Geometry

The slopes from the scatter generated by the smaller-scale, (larger Q) features of the pastes

Table 1 - Slopes of Intensity vs Q log-log Plots with Degrees of Saturation and Limiting Q Values

Saturation (%)	Minimum Q ($Å^{-1}$)	Smaller-Q Slope (larger features)	Intermediate Q ($Å^{-1}$)	Larger-Q Slope (smaller features)	Maximum Q ($Å^{-1}$)
0.0	0.0086	-1.68	0.0796	-3.07	0.2395
0.0	0.0095	-1.74	0.0805	-3.08	0.2205
0.0	0.0095	-1.78	0.0805	-2.99	0.2005
0.0	0.0095	-1.74	0.0805	-3.12	0.2404
0.0	0.0104	-1.77	0.0805	-3.09	0.2404
0.0	0.0095	-1.80	0.0805	-3.09	0.2404
0.0	0.0095	-1.79	0.0805	-3.12	0.2404
0.0	0.0040	-1.77	0.0604	-2.97	0.2207
0.0	0.0044	-1.72	0.0604	-3.02	0.2207
41.1	0.0036	-1.98	0.0200	-2.62	0.2202
41.9	0.0022	-2.01	0.0200	-2.53	0.2202
41.9	0.0041	-2.07	0.0200	-2.52	0.1841
46.5	0.0036	-2.52	0.0401	-2.04	0.0901
53.5	0.0040	-2.48	0.0304	-1.97	0.2207
53.5	0.0037	-2.52	0.0295	-2.01	0.3097
56.8	0.0036	-2.54	0.0401	-1.89	0.2202
56.8	0.0034	-2.29	0.0418	-1.87	0.3100
57.4	0.0040	-2.36	0.0304	-2.06	0.2207
60.1	0.0040	-2.21	0.0304	-1.86	0.2207
65.2	0.0040	-2.19	0.0304	-1.74	0.2207
65.2	0.0031	-2.24	0.0246	-1.81	0.3097
74.8	0.0032	-2.20	0.0247	-1.60	0.1588
74.8	0.0026	-2.18	0.0298	-1.70	0.3100
80.7	0.0032	-2.37	0.0206	-1.68	0.3089
80.7	0.0034	-2.41	0.0199	-1.72	0.2260
81.2	0.0013	-2.39	0.0206	-1.66	0.2488
85.5	0.0032	-2.09	0.0206	-1.36	0.2488
85.5	0.0039	-2.05	0.0199	-1.43	0.2260
88.8	0.0032	-2.12	0.0206	-1.38	0.2189
100.0	0.0061	-2.41	0.0140	-1.42	0.1401
100.0	0.0070	-2.53	0.0140	-1.44	0.1401
100.0	0.0070	-2.51	0.0140	-1.43	0.1401
100.0	0.0033	-2.26	0.0173	-1.48	0.1993

are given in the 5th column of Table 1. The change in these slopes with changing degree of saturation is much greater than in the case of the larger-scale slopes. There is a surface fractal regime (slopes between -2 and -3) for samples with degrees of saturation less than about 50% while wetter samples fall into a mass fractal regime (slopes between 0 and -2). When the appropriate equations are used to convert the slopes to fractal dimensions, the results are as shown in Figure 5.

The size range for the smaller-scale fractal region is also given by the appropriate limiting Q values. Except for the oven dried pastes, the intermediate Q is about 0.03 $Å^{-1}$ while the maximum Q is about 0.2 $Å^{-1}$. Again, this regime also spans about an order of magnitude. These Q's translate to sizes of about 30-200 Å. The minimum size (maximum Q) may be less than 30 Å. This is because data were only taken up to a maximum angular position corresponding to a Q of about 0.2 $Å^{-1}$. Data at greater Q's might show that the smaller-scale fractal region extends to even smaller sizes than 30 Å

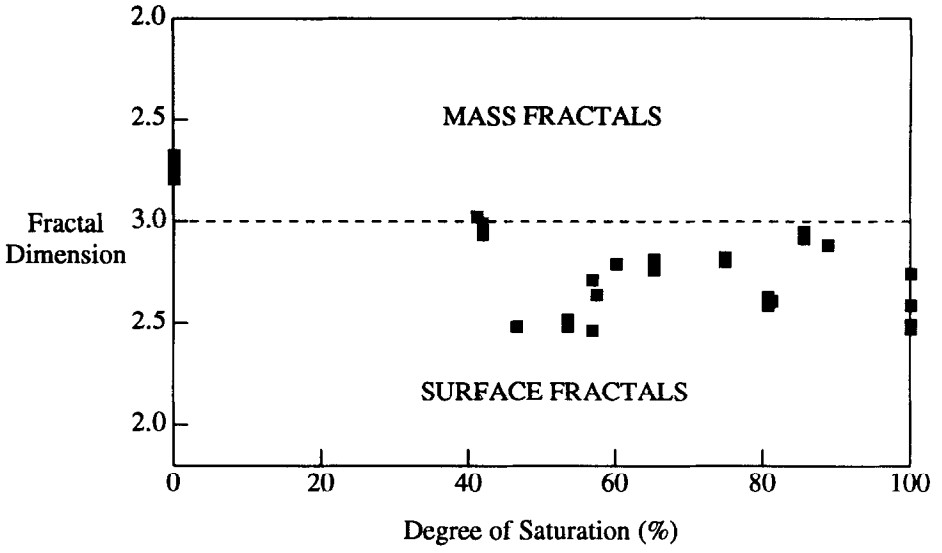

Figure 4 - Fractal Types and Dimensions of Larger-Scale Features

General Geometric Implications

A geometric picture consistent with these findings is as follows. As you view a wet paste at increasingly small scales, you first see a rough, fractal surface of dimension 2.5-3.0. The features on this surface may be as big as 1500 Å or larger. The view remains essentially the same as one increases magnification until one is seeing features as small as about 200 Å. During this increase in magnification, one merely sees smaller features that are similar to the bigger ones. (This is the essence of what is meant by a fractal surface.) This process might be visualized as analogous to flying over a mountain range, and viewing it as your aircraft flies ever

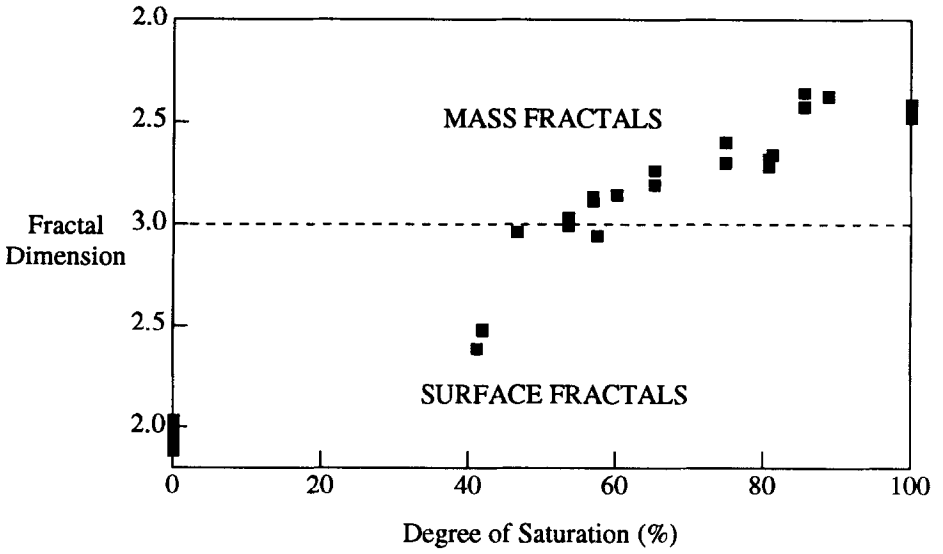

Figure 5 - Fractal Types and Dimensions of Smaller-Scale Features

nearer to the peaks. Finally, the view at these levels of magnification is pretty much the same at any degree of saturation except for complete oven drying.

A still closer view of a wet paste reveals features smaller than about 200 Å. These are imbeded in the coarser fractal surface, and are found to be mass fractals. This might be analogous to finding that mountain outcrops smaller than a certain size do not contain still smaller outcrops similar to those seen at lesser levels of magnification. Instead, they are honeycombed with voids. Further, the larger honeycombed features are, themselves, found to contain even smaller honeycombing. This honeycombing is found to continue down to sizes of about 30 Å. Due to the limitations of the data, one is unable to descern features smaller than this.

Lastly, the view (at magnifications that are great enough to see the mass fractal regime) changes as the paste is dried. At first the mass fractals are seen to coalesce into a denser structure of higher mass fractal dimension as water is removed. Then, at about 50% saturation, the smaller-scale geometry of the pastes becomes fully dense and space filling. At lesser degrees of saturation, the smaller-scale features merge into the rough fractal surface. At these water contents, the surface appears fractal at length scales smaller than 200 Å. Additional drying causes this surface to become ever smoother until the oven dry state is reached. These changes in the smaller-scale geometry are consistent with the fact that one measures a greatly reduced conventional surface area for a dried cement paste.

These changes in both the larger- and smaller-scale geometries are summarized in Figure 6.

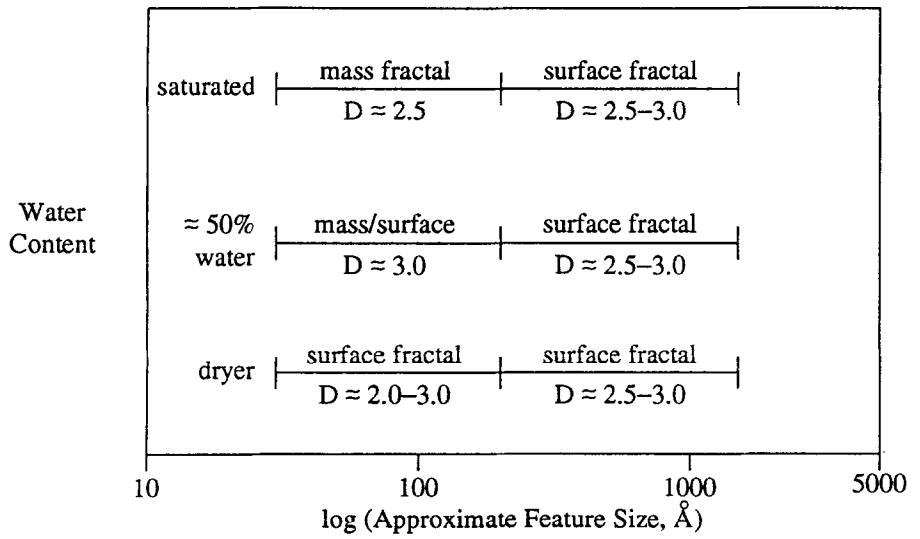

Figure 6 - Changes in Fractal Types and Dimensions with Drying

Transition Between Fractal Types

All of the data show two linear regions in log-log plots such a Figure 3. The point at which the slope changes corresponds to a size that separates one fractal regime from another. For the data here, this size is about 200 Å. Transitions such as these have been found before [4, 5]. In

these cases it has been argued that the change in fractal arrangement represents a change in the solid stemming from differing environments during deposition.

There is no direct evidence that this is the case with the present data. However, it may well be the explanation for these pastes. The two fractal regimes may represent parts of the paste that were formed in different physical locations within the paste or, at different stages of hydration. The present data neither support nor refute this supposition. Additional research is needed to examine this question.

Oven Dried Pastes

The fractal geometry of the completely oven-dried pastes is significantly different from that of pastes with evaporable water present. The larger-scale features (Figure 4) are mass fractals of approximate dimension 2.75. And, the smaller-scale features (Figure 5) are smooth surfaces of fractal dimension 2.0. This is a very different geometric arrangement from that described for samples containing evaporable water.

Virtually all paste that is present in normal concrete has at least some evaporable water. Hence, its geometry is as described under "General Geometric Implications". Oven drying is an experimentally convenient, but highly unusual, state that is often a necessary precursor to microstructural research. The differences in fractal type and dimension of oven dried pastes are further evidence that complete drying produces an altered material. While this alteration may be necessary, its implications, and geometry, should be kept in mind.

Effects of Adsorption vs Desorption

The original preparation of the samples included both adsorption for pre-dried samples and desorption for initially saturated samples. This was done since it was felt that there might be some inherent differences in the resulting microstructures. This does not seem to be the case.

The samples that desorbed water from an initial saturated state do have a larger degree of saturation than the comparable adsorption samples equilibrated at the same relative humidity. This is a result of the hysteresis loop in the sorption isotherm that has been reported often. However, if one compares samples having similar degrees of saturation, rather than coming from similar relative humidities, one cannot distinguish between adsorption and desorption. In other words, samples with similar degrees of saturation have similar fractal geometries regardless of the path they take to reach that degree of saturation.

Some earlier work [6] using small-angle scattering showed that the surface area of a paste could be greatly diminished by complete drying, but was essentially completely recovered upon resaturation. That is, the change was reversible. The findings of the present research merely suggest that this reversibility is more generally true. The pastes' geometries at intermediate degrees of saturation are also fully recoverable after complete drying.

Comparison with Other Research

There have been several prior studies that are, in some aspects, comparable to the present investigation. One study [7] examined the scatter from mature, D-dried pastes prepared at 3 different water/cement ratios, 0.3, 0.4 and 0.6. The scatter was recorded over a more limited range (0.01-0.3 $\mathring{A}^{-1}$) than in the current study. This limited range concealed the two distinct scattering regimes that are reported here. Because of this, the data were grouped into a single range, and used to generate a single surface fractal dimension. It now appears that this dimension represents a composite of a part of the larger-scale regime and the majority of the smaller-scale regime.

Another study [8] involved saturated samples of w/c = 0.5 having ages ranging from 1-28 days. Here again, the range in Q was limited to about 1 order of magnitude (0.015-0.18 $Å^{-1}$). This is roughly the same range as the smaller-scale regime in the present study, and is approximately equivalent to the larger Q region for the saturated sample shown in Figure 3. The authors found that the majority of their data for a 28-day old paste could be attributed to a mass fractal of dimension 2.8 vs the roughly 2.5 of the present study. Their data from the younger samples suggest that there may be another scattering regime at the smallest-scale end of the data. This should be investigated by obtaining high quality data at even larger Q's.

ACKNOWLEDGEMENTS

This work was supported by the NSF Center for Advanced Cement-Based Materials and the authors wish to thank the Center for its support. They also wish to thank the personnel of the Robert R. Wilson Synchrotron Laboratory at Cornell University for their advice and help in performing the scattering experiments. Finally, they wish to thank Paul Schmidt and Peter Pfeifer at the University of Missouri for their help in interpreting the data.

REFERENCES

1. Glatter, O. and Kratky, O., *Small Angle X-Ray Scattering*, Academic Press, New York, (1982)

2. Guinier, A., Fournet, G., Walker, C. and Yudowitch, K., *Small-Angle Scattering of X-Rays*, J. Wiley, New York, pg 2, (1955)

3. Schmidt, P., *Small-Angle Scattering Studies of Disordered, Porous and Fractal Systems*, J. Appl. Cryst., pg 414-435, (1991)

4. Uwaha, M. and Saito, Y., *Fractal-to-Compact Transition and Velocity Selection in Aggregation from Lattice Gas*, J. Physical Soc of Japan, pg 3285-3288, (1988)

5. Garcia-Ruiz, J., Lakhtakia, A. and Messier, R., *Does Competition Between Growth Elements Eventually Eliminate Self-Affinity?*, Speculations in Sc and Tech, pg 60-71, (1992)

6. Winslow, D. and Diamond, S., *Specific Surface of Hydrated Portland Cement Paste as Determined by Small-Angle X-Ray Scattering*, J Amer Ceramic Soc, pg 193-197, (1974)

7. Winslow, D., *The Fractal Nature of the Surface of Cement Paste*, Cement and Concrete Res., pg 817-824, (1985)

8. Kriechbaum, M., Degovics, G., Tritthart, J. and Laggner, P., *Fractal Structure of Portland Cement Paste During Age Hardening Analyzed by Small-Angle X-Ray Scattering*, Prog Colloid Polym Sci, pg 101-105, (1989)